Softer and soft X-rays in macromolecular crystallography

Kristina Djinović Carugo,[a]‡ John R. Helliwell,[b,c] Heinrich Stuhrmann[d,e] and Manfred S. Weiss[f]*

[a]Structural Biology Laboratory, Sincrotrone Trieste in AREA Science Park, I-34102 Basovizza (TS), Trieste, Italy, [b]Department of Chemistry, University of Manchester, Manchester M13 9PL, UK, [c]SRS/CCLRC Daresbury Laboratory, Warrington WA4 4AD, UK, [d]GKSS Forschungszentrum, Geesthacht, Germany, [e]Institut de Biologie Structurale Jean-Pierre Ebel, CEA/CNRS/UJF, 41 rue Jules Horowitz, F-30027 Grenoble, France, and [f]EMBL Hamburg Outstation, c/o DESY, Notkestrasse 85, D-22603 Hamburg, Germany. E-mail: msweiss@embl-hamburg.de

The utilization and the potential of softer and soft X-rays in macromolecular crystallography as well as the challenges associated with the corresponding diffraction experiments and their possible remedies are reviewed.

Keywords: X-ray crystallography; longer wavelengths (1.5–3.0 Å); long wavelengths (>3.0 Å); softer X-rays (1.5–3.0 Å); soft X-rays (>3.0 Å); X-ray absorption; anomalous scattering.

1. Introduction

Historically, macromolecular crystallography (MX) experiments have mostly been conducted using radiation from home sources and copper targets at the Cu K_α wavelength (λ = 1.5418 Å). With the advent and the wider availability of the synchrotron sources around the world, the preferred wavelength among macromolecular crystallographers shifted towards smaller numbers, mainly for two reasons. Firstly, having the higher beam intensities available made up for the reduced scattering at shorter wavelengths (see next paragraph) and, secondly, the use of anomalous scattering for phase determination has become more and more prevalent. Most traditional heavy atoms used for derivatizing macromolecules (Hg, Pt, Au etc.) have their L-absorption edges near λ = 1.0 Å. Similarly, Se, which has become the most popular element for phase determination owing to the straightforward and simple replacement of the natural amino acid Met by the artificial isosteric amino acid Se-Met, has its K-absorption edge close to λ = 0.98 Å. The shorter wavelengths also have the advantage that they are absorbed less by the sample. Thus, data collection and reduction have become even easier, essentially rendering experimental absorption corrections (a practice which is commonly widely used in small-molecule crystallography) obsolete in MX.

However, apart from the mainstream crystallographic work which has been carried out over the past decades, there have also been attempts to widen the wavelength spectrum for MX. The main driving force for this is the attempt to reach X-ray absorption edges of elements which are outside the 'normal' X-ray wavelength range (Fig. 1). The groups of John Helliwell (Helliwell *et al.*, 1993), Roger Fourme (Schiltz *et al.*, 1997) and Paul Tucker (personal communication) have explored the short wavelengths down to λ = 0.3 Å, reaching the K-edge of iodine and xenon for phase determination, while Heinrich Stuhrmann and colleagues (Lehmann *et al.*, 1993; Stuhrmann *et al.*, 1995, 1997; Behrens *et al.*, 1998; Carpentier *et al.*, 2000)
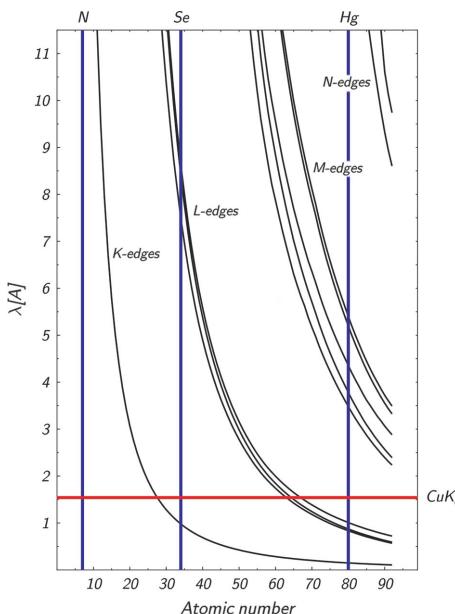

Figure 1
K, L, M and N-absorption edges of the first 92 elements. For reference the vertical lines at atomic numbers 7 (for nitrogen), 34 (for selenium) and 80 (mercury) are also given, as is the Cu K_α wavelength of 1.5418 Å as a horizontal line.

‡ Current address: Max F. Perutz Laboratories, University Departments at Vienna Biocenter, Institute for Theoretical Chemistry and Molecular Structural Biology, University of Vienna, Campus Vienna Biocenter 6/1, Rennweg 95b, A-1030 Vienna, Austria.

Table 1
Operational nomenclature and definition of X-ray wavelength ranges.

Description	Wavelength range (Å)	Energy range (keV)
Short wavelengths (hard X-rays)	<0.7	>17.0
Normal wavelengths (normal X-rays)	0.7–1.5	8.0–17.0
Longer wavelengths (softer X-rays)	1.5–3.0	4.0–8.0
Long wavelengths (soft X-rays)	>3.0	<4.0

have gone in the other direction and used long wavelengths up to $\lambda = 6.0$ Å with the aim of obtaining anomalous diffraction information from the naturally present phosphorus and sulfur atoms in biological macromolecules. However, since rather few beamlines for MX are operated at either $\lambda = 0.3$ Å or at $\lambda = 6.0$ Å, and since the wavelength used restricts d_{min} to, at best, $\lambda/2$, neither the short-wavelength experiments nor the long-wavelength experiments, respectively, have been followed much.

Very recently, *i.e.* in the past two or three years or so, the use of the intermediate wavelength range $\lambda = 1.5$–3.0 Å (also termed longer X-ray wavelengths or softer X-rays; for definitions see also Table 1) has gained quite some popularity in MX. This can be rationalized by looking at the anomalous scattering lengths of all elements at the two wavelengths $\lambda = 1.0$ Å and $\lambda = 2.0$ Å (Fig. 2). It is evident that there are three regions among the 92 elements where the longer wavelength provides a clear advantage over the shorter wavelength. These regions constitute the light elements P, S, Cl, Ca *etc.*, the medium heavy elements I, Xe and Cs, and the very heavy elements Hg and heavier in the periodic system. In addition to providing an increased anomalous scattering signal from the

elements mentioned, these longer wavelengths possess the additional advantage that experimental difficulties are certainly less severe than when going to the long wavelengths. It could even be shown (Helliwell, 1984; Cianci *et al.*, 2001; Weiss, Sicker, Djinović Carugo & Hilgenfeld, 2001) that these longer wavelengths can be reached on some synchrotron beamlines without making any modifications to the beamline. This certainly opened the possibility for a more routine use of them in MX. For home laboratories, a chromium target delivering a wavelength of $\lambda = 2.29$ Å was discussed more than 40 years ago by Blow (1958), but apart from a few scattered experiments (*e.g.* Anderson *et al.*, 1996; Kwiatkowski *et al.*, 2000) it has never really caught on until recently, when the Molecular Structure Corporation entered the diffraction equipment market with a rotating anode made of chromium (Yang *et al.*, 2003).

In this review we will give an overview of the use of softer and soft X-rays in MX and the potential associated with it as well as the experimental challenges and their possible remedies.

2. Theoretical background

Factors which may influence the choice of the wavelength for a diffraction experiment are the scattering efficiency, radiation damage, the spectral distribution of the source, the monochromator limits, the detector response and, most of all, the purpose of the experiment. If, for instance, the maximum anomalous signal is sought, one needs to take the wavelength dependence of the anomalous scattering lengths into account and very often the choice of 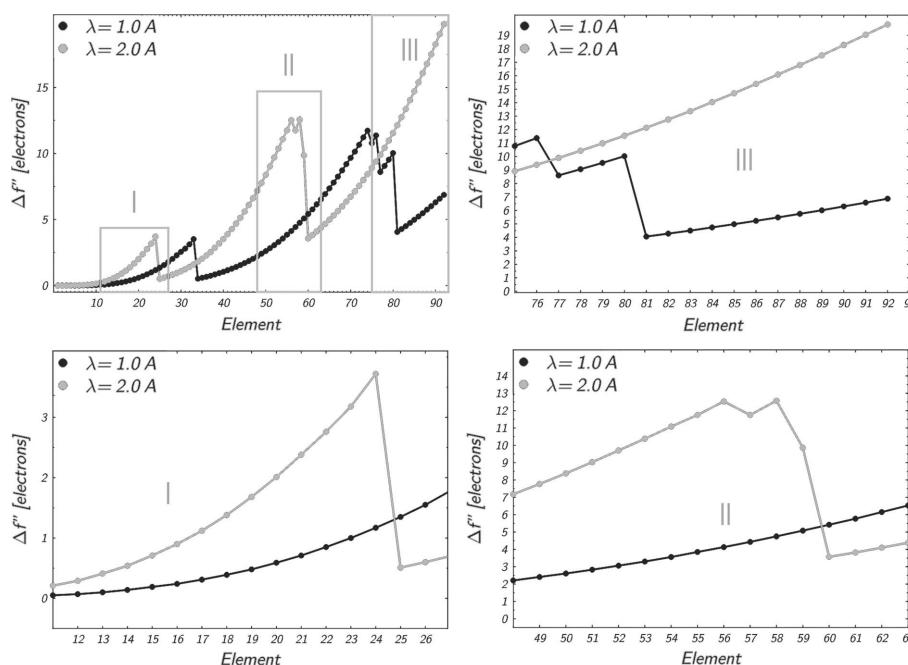the wavelength is dependent on which elements are present in the crystal and whether an absorption edge of one of these elements can be reached (Fig. 1). If no absorption edge can be reached, the situation becomes slightly more complicated (see below). In the following paragraphs a few theoretical aspects have to be introduced. A more detailed discussion including the derivation of the relevant equations can be found by Arndt (1984), Polikarpov (1997), Polikarpov *et al.* (1997) and Murray *et al.* (2004).

The total atomic form factor is written as

$$f = f_0 + \Delta f' + i\Delta f''. \quad (1)$$

The optical theorem relates the total absorption cross section σ to the imaginary part of the atomic form factor, which is also called the anomalous or resonant atomic scattering length $\Delta f''$,

$$\sigma = 2\lambda \Delta f'', \quad (2)$$

Figure 2
Anomalous scattering length ($\Delta f''$) values in units of electrons at $\lambda = 1.0$ Å (black) and $\lambda = 2.0$ Å (grey) for the first 92 elements (top left), for elements 11–27 (bottom left), 48–63 (bottom right) and 75–92 (top right).

where $\Delta f''$ is expressed in units of the scattering length of one electron. At wavelengths not too close to an X-ray absorption edge, $\Delta f''$ increases with λ^2, therefore the total cross section increases with λ^3. The linear absorption coefficient μ can then be calculated from the total absorption cross section using (3),

$$\mu = N\sigma, \tag{3}$$

with N being the number of atoms per unit volume. Consequently, the relative decrease of the intensity I/I_0 owing to absorption is

$$I/I_0 = \exp(-\mu x), \tag{4}$$

where x is the path length of the X-ray beam in the specimen.

The integrated scattered X-ray intensity of a crystal as a function of the wavelength λ is given in (5) (see also Arndt, 1984),

$$I \propto \lambda^3 x^3 \exp(-\mu x)/\sin(2\theta), \tag{5}$$

with 2θ being the scattering angle. At small angles 2θ, $\sin(2\theta)$ can be approximated by λ/d and (5) reduces to

$$I \propto \lambda^2 x^3 \exp(-\mu x). \tag{6}$$

This shows that scattering increases with λ^2 but at the same time absorption increases with λ^3. It has therefore been argued by Helliwell (1993) and Teplyakov et al. (1998) that at λ [Å] $= (3/x \text{ [mm]})^{1/3}$ the scattering efficiency is maximal, which would call for longer wavelengths being more suitable for smaller crystals. However, this argument is only valid in the absence of radiation damage to the sample. In case the purpose of the experiment is to obtain the maximum anomalous signal, the wavelength dependence of $\Delta f''$ needs to be taken into account (see above). Remote from any absorption edge, longer wavelengths will in many cases provide larger signals (Fig. 2), but data collected at longer wavelengths will also be contaminated with noise resulting from absorption effects. Since in MX absorption is usually only treated implicitly at the scaling stage, it must be expected that one has to compromise at some wavelength where the noise resulting from absorption effects does not overwhelm the signal. Preliminary studies in this context (Weiss, Sicker & Hilgenfeld, 2001; Mueller-Dieckmann et al., 2004) point towards wavelengths of about 1.9–2.3 Å yielding the highest anomalous signal-to-noise ratio. It is feasible, however, that more sophisticated data-collection procedures and/or data-reduction approaches may shift this optimum wavelength towards higher numbers, which would provide even higher anomalous effects.

3. What is possible with softer and soft X-rays?

As already mentioned above and shown in Fig. 2, softer X-rays at $\lambda = 2.0$ Å provide a larger anomalous signal for many of the first 92 elements than X-rays at $\lambda = 1.0$ Å. This immediately leads to their potential use. One of the early applications of softer X-rays in MX was the successful identification of Mn^{2+} in the structure of pea lectin by Helliwell and colleagues (Einspahr et al., 1985) based on diffraction data collected at the K-edge of Mn ($\lambda = 1.896$ Å). Similarly, So Iwata and his colleagues (Ferreira et al., 2004) managed to establish the architecture of the photosynthetic oxygen-evolving center consisting of Mn^{2+} and Ca^{2+} ions by collecting diffraction data at wavelengths on both sides of the Mn K-edge. The identification of ions such as Cl^- or Ca^{2+} and their distinction from others such as Na^+ or from water molecules has also been reported a number of times (Weiss, Sicker, Djinović Carugo & Hilgenfeld, 2001; Weiss et al., 2002; Kuettner et al., 2002; Sekar et al., 2004).

Apart from the identification or validation of ligands or ions etc., the anomalous signal of metal ions which are present in the native protein can also be easily and efficiently used for ab initio phase determination. About 30% of all proteins are metalloproteins, and many of them contain first-row transition metals. Among the metals exhibiting a K-absorption edge in the longer wavelength region (Fig. 1) are Cr, Mn, Fe and Co with K-edges at $\lambda = 2.070$, 1.896, 1.743 and 1.608 Å, respectively. These metals are in principle all amenable for a MAD or SAD experiment. The pioneer experiment reporting the successful use of the anomalous signal of iron was to our knowledge performed on haemerythrin (Smith et al., 1983) using Cu K_α radiation, where the anomalous scattering length of Fe amounts to about three electrons. Closer to the K-absorption edge of Fe, $\Delta f''$ increases to about four electrons (not taking the white line into account) but, in order to make maximum use of this, access to synchrotron radiation is mandatory. Owing to the scarcity of synchrotron beamlines at that time and owing to the fact that the method was not widely spread across the community, it took until 1988 before similar experiments on ferredoxin (Murthy et al., 1988) and on lamprey haemoglobin (Hendrickson et al., 1988) were undertaken. Among the four bio-metals listed above, iron is certainly and by far the most prominent and since then has been used in increasingly challenging experiments, an example being the structure determination of the cytochrome bc1 complex (Xia et al., 1997). To our knowledge, none of the other three metals have so far been used successfully in a MAD experiment (for a review, see Hendrickson, 1999), with the one exception that Dauter and colleagues have shown that a Mn-SAD experiment is also feasible (Ramagopal et al., 2003).

An additional important advantage of softer X-rays is that they provide the possibility of phase determination from the light atoms alone. The first successful example was the determination of the structure of crambin based on the anomalous scattering of the native sulfur atoms using Cu K_α radiation (Hendrickson & Teeter, 1981). Almost 20 years later, Zbyszek Dauter and colleagues rediscovered this approach in the structure determination of the model protein lysozyme (Dauter et al., 1999). Much of the renewed interest in using the anomalous scattering of sulfur atoms for phase determination can be traced back to the Dauter et al. (1999) paper, although B. C. Wang had postulated as early as 1985 (Wang, 1985) that the method should in principle be generally applicable. Dauter et al. (1999) used synchrotron radiation at $\lambda = 1.54$ Å, but some of the subsequent work was also performed on home

sources using Cu K_α radiation (Yang & Pflugrath, 2001; Debreczeni *et al.*, 2003; Weiss, 2001). The photoprotein obelin was to our knowledge the first protein, whose structure was determined *de novo* by sulfur anomalous scattering at a longer wavelength (λ = 1.74 Å) (Liu *et al.*, 2000). Other recent examples of successful structure determination by sulfur or other light-atom anomalous scattering constitute both model proteins such as thermolysin at various wavelengths between 1.5 and 2.64 Å (Weiss, Sicker & Hilgenfeld, 2001), trypsin at λ = 1.54 Å (Yang & Pflugrath, 2001), trypsin, insulin and thaumatin at λ = 1.54 Å (Debreczeni *et al.*, 2003) and glucose isomerase and xylanase at λ = 1.54 Å and 1.74 Å, respectively (Ramagopal *et al.*, 2003); also real-life cases such as the C_1 subunit of α-crustacyanin at λ = 1.77 Å (Gordon *et al.*, 2001), the IGF2R fragment at λ = 1.77 Å (Brown *et al.*, 2002), the CAP-Gly domain at λ = 1.74 Å (Li *et al.*, 2002), tryparedoxin at λ = 1.77 Å (Micossi *et al.*, 2002), the bubble protein at λ = 1.54 Å (Olsen *et al.*, 2004) and lobster apocrustacyanin A1 (Cianci *et al.*, 2001). In the latter case, the structure determination was based on a Xe derivative, but the anomalous scattering of the S atoms present in a diffraction data set collected at λ = 2.00 Å proved essential to establish the hand of the xenon substructure. Since the obtainable anomalous signal from the light atoms is usually small, diffraction data must typically be collected to very high redundancy in order to increase the signal-to-noise ratio (Dauter & Adamiak, 2001; Weiss, 2001). This leads to an inevitable conflict with the advent of radiation damage. However, even this can be turned into an advantage as was postulated by Ravelli *et al.* (2003), who proposed the method of radiation-damage-induced phasing (RIP), in which the isomorphous differences introduced into the structure by radiation damage form the basis for phase determination. It is conceivable that a combination of the RIP method with long-wavelength sulfur anomalous scattering may have the potential to develop into a standard phase-determination method. The recent successful *de novo* structure determination of the γ-subunit of dissimilarity sulfite reductase at λ = 1.90 Å (Weiss *et al.*, 2004) constitutes both the proof-of-principle as well as the first real-life example of this.

The next candidate experiments which would benefit from softer X-rays are crystal derivatizations with the medium heavy elements. Using either the pressure derivatization with Xe, the quick-soaking of protein crystals with I^- (Dauter *et al.*, 2000), with I_2/I^- (Evans & Bricogne, 2002, 2003; Evans *et al.*, 2003) or with Cs^+ solutions, useful derivatives of protein crystals can be obtained and the increased anomalous signal available at longer wavelengths provides advantages in phase determination. As a matter of fact, the very first anomalous scattering MX experiment at longer wavelengths was the study on a caesium derivative of the polypeptide gramicidin (Phillips & Hodgson, 1980). The experiment was conducted at the L(III)-edge of Cs (λ = 2.47 Å), which has a strong white line, very much similar to that of the rare earth ions. Further example experiments are the structure determination of apocrustacyanin A1 (two molecules of 20 kDa each in the asymmetric unit) as mentioned above (Cianci *et al.*, 2001), and also the test experiments on a series of different wavelengths

performed on a xenon derivative of porcine pancreatic elastase (Mueller-Dieckmann *et al.*, 2004).

Last but not least, the very heavy elements such as U will also exhibit a much larger anomalous signal when the diffraction data are collected at longer wavelengths. An extension of the quick-soaking method of Dauter and colleagues to the use of UO_2^{2+} ions would therefore be an attractive option. In pilot experiments (unpublished data) it was shown by one of the authors (MSW) that this approach is indeed feasible. If the M-edges of U, which are between λ = 2.9 and 3.5 Å, could be reached it was calculated by Hendrickson & Ogata (1997) that one single U atom would actually be sufficient to obtain phases for a molecule as large as the whole ribosome. This is due to an intense white line at the M(V)-edge of U, which can give rise to an anomalous scattering length $\Delta f''$ of approximately 110 e⁻. Following up on this, Hendrickson and colleagues (Liu *et al.*, 2001) conducted a successful feasibility experiment on NSLS beamline X4C (Brookhaven, USA) at the uranium M(IV)-edge at λ = 3.3 Å. The experiment was conducted in the dark as the image-plate cover had to be removed to avoid absorption in the detector front window. Independently, the large $\Delta f''$ value at the uranium M(V)-edge at λ = 3.5 Å was confirmed experimentally at the ESRF (Grenoble, France) in a MAD study on a uranium derivative of lysozyme (Chesne, 2002).

Other potential experiments which could obviously benefit from the use of longer wavelengths are the multiple-wavelength anomalous solvent contrast experiments performed by Fourme and colleagues and Kratky and colleagues (Fourme *et al.*, 1995; Ramin *et al.*, 1999; Sauer *et al.*, 2002), which complement the methods of chemical or isotopical contrast variation in X-ray and neutron crystallography, respectively, the validation of molecular replacement solutions by a technique called MR-SAD (Schuermann & Tanner, 2003), or single-molecule scattering (Miao *et al.*, 2001; Helliwell, 2004).

4. Synchrotron beamlines with softer and soft X-ray capability

A survey of MX beamlines at European synchrotron facilities shows that softer wavelengths are accessible at several operational beamlines (Table 2). A clear trend towards the coverage of longer wavelengths can be observed in the designs of beamlines currently under construction, in the commissioning phase or in the planning stage. This indicates that both the general user community as well as the beamline staff have started to appreciate a series of advantages offered by the possibility of utilizing softer and soft X-rays for MX. As an example for a beamline optimized for softer X-rays, the new MX beamline 10 currently being built at the SRS will be discussed in more detail in the next section.

5. A new MX beamline optimized for softer X-rays at the SRS in Daresbury

A joint effort of research groups from several universities in the northwest of the UK, two major pharmaceutical compa-

Table 2
Beamlines for MX at synchrotron facilities worldwide.

Facility	Web page	Beamline	Wavelength range (Å)	Energy range (keV)	Status†
Europe					
ANKA	hikwww1.fzk.de/anka/	PX	0.62–3.10	20.0–4.0	OP
BESSY	www.bessy.de	ID14-1	0.75–2.48	16.5–5.0	OP
		ID14-2	0.75–2.48	16.5–5.0	OP
		ID14-3	0.90	13.8	COM
DESY/EMBL	www.embl-hamburg.de	X31	0.70–1.80	17.7–6.9	OP
		X11	0.81	15.3	OP
		X12	0.72–2.07	17.2–6.0	COM
		X13	0.80	15.5	OP
		BW7A	0.77–1.80	16.1–6.9	OP
		BW7B	0.83	14.9	OP
DESY/MPG	www-hasylab.desy.de	BW6	0.65–2.10	19.1–5.9	OP
DIAMOND	www.diamond.ac.uk	I02	0.50–2.50	24.8–5.0	CON
		I03	0.50–2.50	24.8–5.0	CON
		I04	0.50–2.50	24.8–5.0	CON
		SoftX	?	?	PL
ELETTRA	www.elettra.trieste.it	XRD1	0.50–3.1	24.8–4.0	OP
		XRD2	0.65–3.1	19.1–4.0	CON
ESRF	www.esrf.fr	ID14-1	0.93	13.3	OP
		ID14-2	0.93	13.3	OP
		ID14-3	0.93	13.3	OP
		ID14-4	0.86–1.29	14.4–9.6	OP
		ID23-1	0.60–2.88	20.7–4.3	OP
		ID23-2	0.89	13.9	CON
		ID29‡	0.35–1.30/ 0.80–2.40	35.4–9.5/ 15.5–5.2	OP
		BM14	0.70–1.80	17.7–6.9	OP
		BM16	0.73–2.00	17.0–6.2	OP
LURE	www.lure.u-psud.fr	DW32	1.00	12.4	CL
MAXLAB	www.maxlab.lu.se	I911-1	1.10	11.3	CON
		I911-2	1.03	12.0	CON
		I911-3	0.70–1.80	17.7–6.9	CON
		I911-4	0.91	13.6	CON
		I911-5	0.97	12.8	CON
		I711	0.80–1.60	15.5–7.7	OP
SLS	sls.web.psi.ch	PX1	0.71–2.48	17.5–5.0	OP
		PX2	0.62–2.48	20.0–5.0	CON
SRS	www.srs.ac.uk	9.5	0.65–2.00	19.1–6.2	OP
		9.6	0.87	14.3	OP
		7.2	1.40–2.60	8.9–4.8	OP
		10.1	0.9–2.5	13.8–5.0	COM
		14.1§	1.20/1.49	10.3/8.3	OP
		14.2§	0.98/1.20	12.7/10.3	OP
SOLEIL	www.synchrotron-soleil.fr	ID10C	0.73–3.5	17.0–3.5	PL
		ID10M	0.73–3.1	17.0–4.0	PL
North and South America					
ALS	www.als.lbl.gov	4.2.2	0.69–2.1	18.0–6.0	OP
		5.0.1	1.0	12.4	OP
		5.0.2	0.89–3.5	14.0–3.5	OP
		5.0.3	1.0	12.4	OP
		8.2.1	0.73–2.5	17.0–5.0	OP
		8.2.2	0.73–2.5	17.0–5.0	OP
		8.3.1	0.69–5.2	18.0–2.4	OP
		12.3.1	0.73–2.25	17.0–5.5	OP
APS	www.aps.anl.gov	8-BM	0.84–1.9	14.7–6.5	COM
		14-BM-C	0.83–1.55	14.9–8.0	OP
		14-BM-D	0.69–1.77	18.0–7.0	OP
		14-ID	0.71–1.9	17.5–6.5	OP
		17-BM	0.62–2.1	20.0–6.0	OP
		17-ID	0.73–2.1	17.0–6.0	OP
		19-BM	0.92–2.1	13.5–6.0	OP
		19-ID	0.64–1.9	19.5–6.5	OP
		22-BM	0.62–2.1	20.0–6.0	OP
		22-ID	0.62–2.1	20.0–6.0	OP
		31-ID	0.50–2.8	25.0–4.5	COM
CAMD	www.camd.lsu.edu	GCPCC	?	?	CON
CHESS	www.chess.cornell.edu	A1	0.95	13.1	OP
		F1	0.92	13.5	OP
		F2	0.77–1.57	16.0–7.9	OP
CLSI	www.cls.usask.ca	08-ID.1	0.69–1.9	18.0–6.5	CON

nies (AstraZeneca and Astex-Technology) and the CCLRC Daresbury Laboratory is currently underway building beamline 10, a new MAD beamline at the SRS on a new high-field multipole wiggler source. Beamline 10 is dedicated to MAD techniques, operating in the 0.9–2.5 Å wavelength range, or the 13.8–5.0 keV photon energy range (Table 2). In order to meet the requirements of speed and tunability necessary for this project, a new 2.4 T tenpole wiggler had to be developed by the Daresbury project team staff. The optical system contains a Rh-coated collimating mirror, a double-crystal Si(111) monochromator with horizontal sagittal focusing, and finally a second Rh-coated mirror for vertical focusing. The monochromatic beam is optimized through a 200 µm × 200 µm collimator. The double-crystal monochromator guarantees rapid tunability and high-energy resolution allowing data to be collected from small weakly diffracting crystals over a wide range of wavelengths. Since SRS is a 2 GeV storage ring, the beam intensity at longer wavelengths is especially strong. In order to make maximum use of this, the beamline Be-window thickness has been minimized. Moreover, to encourage longer wavelength data collection the detector can be tilted to a maximum angular coverage of $2\theta = 110°$. A full paper on the beamline discussed here will be presented separately at a later stage (Cianci *et al.*, 2005).

6. Experimental difficulties and potential solutions

The collection of diffraction data at wavelengths longer than those routinely employed at both synchrotron and home X-ray sources is complicated by a number of experimental difficulties. Purely technical hitches include the physical monochromator limits, the limitations caused by the energy spectrum of synchrotron sources or simply the lower detector efficiency. Impediments inherently connected to the experiments include the increased absorption of X-rays at long wavelengths, the scatter of primary and secondary beams by air, the larger diffraction angles and the occurrence of the third harmonic reflections when Si(111) is used as a monochromator. In the absence of an

Table 2 (continued)

Facility	Web page	Beamline	Wavelength range (Å)	Energy range (keV)	Status†
LNLS	www.lnls.br	D03B	1.0–2.0	12.4–6.2	OP
NSLS	www.nsls.bnl.gov	X4A	0.41–3.1	30.0–4.0	OP
		X4C	0.62–1.77	20.0–7.0	OP
		X6A	0.62–1.77	20.0–7.0	OP
		X8C	0.65–2.48	19.0–5.0	OP
		X9A	0.84–1.85	14.8–6.7	OP
		X9B	0.90–2.48	13.8–5.0	OP
		X12B	0.95–1.61	13.1–7.7	OP
		X12C	0.95–1.55	13.0–8.0	OP
		X25	0.4–4.1	28.0–3.0	OP
		X26C	?	?	OP
SSRL	www-ssrl.slac.stanford.edu	BL1-5	0.77–2.1	16.0–6.0	OP
		BL7-1	1.08	11.5	OP
		BL9-1	0.73–1.0	17.0–12.4	OP
		BL9-2	0.60–2.1	20.7–6.0	OP
		BL11-1	0.82–1.20	15.1–10.3	OP
		BL11-3	?	?	CON
Asia, Australia					
Australian Synchrotron	www.synchrotron.vic.gov.au	1	0.54–6.2	23.0–2.0	CON
		2	0.62–2.25	20.0–5.5	CON
NSRL	www.nsrl.ustc.edu.cn	U7B	1.0–3.0	12.4–4.1	CON
Photon Factory	pfwww.kek.jp	BL-5	?	?	?
		BL-6A	0.80–1.8	15.5–6.9	OP
		BL-6B	0.90–1.8	13.8–6.9	OP
		BL-6C	0.90–1.8	13.8–6.9	OP
		AR-NW12	?	?	?
SPring-8	www.spring8.or.jp	BL26B1	0.73–2.1	17.0–6.0	OP
		BL26B2	0.73–2.1	17.0–6.0	OP
		BL40B2	0.69–1.77	18.0–7.0	OP
		BL41XU‡	0.34–0.65/ 0.7–1.9	37.0–19.0/ 17.5–6.5	OP
		BL44XU	0.77–1.4	16.0–9.0	OP
		BL44B20	0.4–2.1	30.0–6.0	OP
		BL45XU	?	?	?

† OP: in operation; COM: commisioning stage; CON: under construction; PL: planning stage; CL: closed. ‡ Two wavelength ranges possible. § Two fixed wavelength settings possible.

Table 3
Helium and air attenuation lengths at different wavelengths.

The lengths given denote the distance in the medium, after which the X-ray beam is attenuated to 1/e. Data were taken from the web page of the E. O. Lawrence Berkeley National Laboratory (http://www-cxro.lbl.gov).

Wavelength (Å)	Energy (eV)	Air (mm)	Helium (mm)
0.50	24798	19182	317371
1.00	12398	3172	314079
1.50	8266	925	284491
2.00	6199	384	219613
2.50	4960	196	147483
3.00	4133	113	93712
3.50	3542	72	59503
4.00	3100	54	38754
4.50	2755	38	26171
5.00	2480	28	18359

and secondary photons, and therefore lower the exposure times of the sample to X-rays. Lowering the scattering cross section will on the other hand decrease the background level and therefore increase the signal-to-noise ratio of the diffraction images. The construction of the helium-purged beam path (HePBP) implemented at Elettra (Polentarutti *et al.*, 2004) was driven by the fact that the scattering and absorption of X-rays by helium is by two to three orders of magnitude lower than by air (Table 3, Fig. 3). The HePBP matches the requirements mentioned above by enclosing the complete path of the primary beam (from the last beamline Kapton window to the crystal sample) and of the secondary beams region (from the sample to the detector surface), avoiding any window along the beam path (Fig. 4). Moreover, it allows the use of only slightly modified conventional cryo-cooling instrumentation for sample mounting and data collection.

For diffraction experiments at longer wavelengths of up to 6.0 Å, the requirements are even more strict. Whereas the diffraction experiments at Elettra carried out using softer X-rays certainly benefit from the reduced absorption in the HePBP, the use of helium becomes an absolute requirement when trying to utilize the soft X-rays at wavelengths greater than 3.0 Å. At beamline ID01 at the ESRF (Grenoble, France) the X-ray optics allow the use of wavelengths between 0.3 and 5.9 Å, which would in principle allow even the *K*-edge of P to be reached (Carpentier *et al.*, 2002; Biou *et al.*, 2005). Heinrich Stuhrmann and his colleagues have taken an approach similar to the one which was realised in the Elettra design of the HePBP. The whole diffraction experiment has to be carried out in a helium atmosphere (Carpentier *et al.*, 2002), which requires that the detector also be made part of the assembly. The system at ID01 includes a cylindrical detector set-up, which has the additional advantage that diffraction angles of up to 150° can be recorded, roughly corresponding to a resolution of $d_{min} = 3.1$ Å at $\lambda = 5.9$ Å. Test experiments on a crystal of lysozyme at wavelengths between 2.7 Å and 5.7 Å and diffraction angles between −15° and +75° showed that the system performance is promising. However, in the present assembly the detector can only be read out offline, which makes routine use difficult and tedious. A possible alternative to a cylindrical detector could be the use of a swing-out (2θ) angle for the detector, but this in turn would almost certainly lead to an increase in the total data-collection time. In addition to the requirements for the diffractometer and the detector, the crystal must be made accessible to soft X-rays, which requires the removal of the solvent layer from the
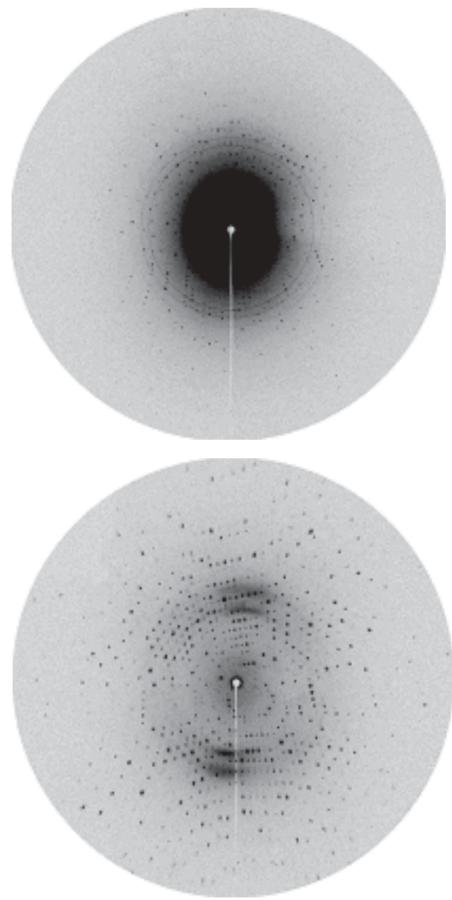
experimental or an analytical absorption correction, the increased absorption certainly represents the most severe problem.

In order to reduce the strong absorption of softer and soft X-rays in the air, the diffractometer has to be adapted in a way as to keep both primary and secondary beams in a lower absorbing and scattering atmosphere. The reduction of the absorption cross section will decrease the losses of primary

Figure 3

Visual comparison between diffraction images collected at 2.60 Å wavelength in air (top) and helium (bottom) atmospheres. The two images were collected from a crystal of porcine pancreatic elastase at the same sample–detector distance (36 mm) and the same exposure time at the XRD1 beamline at Elettra.

Figure 4

The helium-purged beam path (HePBP) at the XRD1 beamline at Elettra. (*a*) Schematic representation of the HePBP. The helium atmosphere reaches from the end of the beamline vacuum system all the way to the detector without any windows in the path. Helium is supplied into the system by the use of a modified cryostream cooler which uses gaseous He cooled to liquid-nitrogen temperature for cooling the crystal. The collimation system C (containing the slit system, the collimator and the ionization chambers IC1 and IC2 for table alignment) is also part of the HePBP. (*b*) Photograph showing the opened HePBP. A plastic PVC box encloses the rotation axis, the collimation system C and the modified cryostream cooler. A flexible rubber bellow mounted on the MarCCD165 detector is pressed against the PVC enclosure by the detector itself, when the sample-to-detector distance is in the range between 35 and 80 mm, ensuring a helium atmosphere produced and maintained by the cryostream cooler. A valve at the bottom of the box allows a regulation of the pressure within the HePBP. (More photographs of the HePBP mounted on the Marresearch standard base can be seen on the web pages of the Structural Biology Laboratory at Elettra, http://www.elettra.trieste.it/organisation/experiments/laboratories/structural_biology/softxrays/).

crystal sitting in the loop. Instead of keeping the crystal in a loop, a better approach is to lay it on a 6 µm thin Hostaphan (polypropylene) foil, the size of which should be adapted to the dimensions of the crystal (Stuhrmann, 1997).

Since every window in a beamline absorbs X-rays, ideas have been developed to construct a beamline free of windows (windowless beamline). A schematic view of a windowless beamline optimized for soft X-ray diffraction is shown in Fig. 5. All optical elements would be, as usual, in an evacuated environment. Windowless operation may be allowed once the pressure in the front-end housing of the diffractometer is well below 10^{-5} bar (chamber R in Fig. 5*a*). This is not an unusual requirement, it can be easily achieved by differential pumping and, as a matter of fact, it is the usual practice for instance at beamline ID01 of the ESRF (Grenoble, France). The size of the housing determines the time for evacuation. At ID01, one to two hours are needed for the evacuation of the large chamber, whereas the small volume of the camera shown in Fig. 5 should reach the necessary pressure level in a few minutes. Protocols for handling protein crystals in an evacuated environment were developed in the 1990s (Stuhrmann *et al.*, 1995, 1996; Stuhrmann, 1997; Thomas, 1997; Trame,
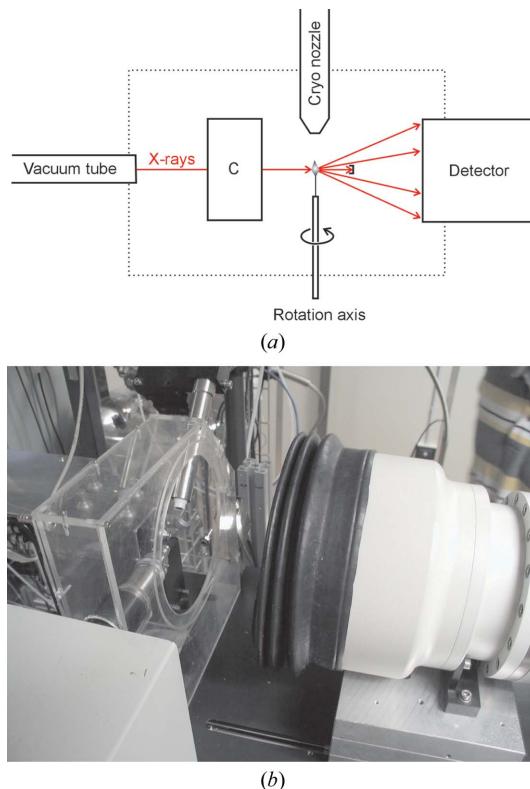
1997). The cooling of the sample in an evacuated environment is performed most conveniently using Peltier elements arranged as a cascade, which can achieve a temperature of 160 K. It is essential to have a dry atmosphere inside the camera, as formation of ice will start at temperatures below 200 K. The vacuum tightness of the camera is important, as humid air entering through leaks is the reason for frost, even at a pressure below 10^{-5} bar. The cold protein crystal is in an environment of cold nitrogen, enclosed in a plastic cell of diameter 3 mm and wall thickness 10 µm. A windowless beamline for fully optimized softer X-ray diffraction experiments is now also being considered at the Diamond Light Source (Duke, 2004).

With respect to diffraction data reduction, it should in principle be possible to utilize the currently available software to process the data collected at longer and long wavelengths. However, it could be shown that, although the current integration software seems appropriate, the scaling software has
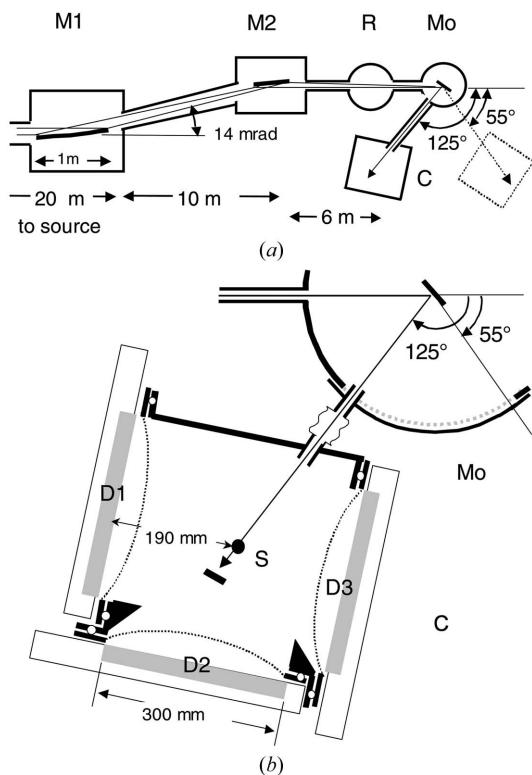

Figure 5
Schematic drawing (not to scale) of a windowless beamline designed specifically for soft X-ray diffraction. The design is close to that which existed at beamline A1 of HASYLAB (DESY, Hamburg, Germany) until 1996. There are no windows between the source and the detector. The toroidal mirror M1 at about 20 m distance from the source is the first focusing element in the beam (the second is a focusing capillary between the monochromator crystal and the sample, not shown). Using a grazing angle of $6°$ the gold-coated surface reflects X-rays with $\lambda > 1.0$ Å. The second plane mirror M2 contains both a gold and a quartz band. The quartz surface will reflect X-rays with $\lambda > 2.4$ Å onto the monochromator Mo. This pre-monochromatization is chosen in such a way that the monochromator crystal will reflect the fundamental wavelength only. The chamber R may contain XY slits *etc.* Its function is also that of a buffer, if the vacuum is lost accidentally in the monochromator box or the camera. The pressure limit in R is 10^{-5} mbar. In the monochromator box Mo, where the pressure should not exceed 10^{-4} mbar, various monochromator crystals (Si111, Ge111, InSb111 and Si311) are held resident. The latter crystal is used when reference measurements at shorter wavelengths are required. As there is only one monochromator crystal, the diffractometer has to follow the direction of the beam, which changes with the wavelength. In order to cover the range $55° < 2\theta < 125°$ the cylindrical monochromator box has to have a movable exit slit. With such a system, wavelengths between 1.25 Å and 6.9 Å, free of higher harmonics, are possible. The camera C has to be kept at a pressure below 10^{-2} mbar. It contains three area detectors of 300 mm × 300 mm surface at a distance of 190 mm to the sample S covering scattering angles from $-109°$ to $+145°$, with two gaps of about $15°$. The out-of-plane angular range is $\pm38°$. Thus, such a detector system can cover 38% of the unit sphere. The large composite detector windows are described by Scholl *et al.* (1995). An improvement over this could be a detector system comprised of cylindrically bent imaging plates which can cover up to about two-thirds of the unit sphere.

serious deficiencies (Weiss, Sicker, Djinović Carugo & Hilgenfeld, 2001; Mueller-Dieckmann *et al.*, 2004). Whereas up to a wavelength of 1.7 Å standard current scaling protocols can be used, between 1.7 and 2.3 Å a more elaborate three-dimensional scaling protocol or the use of an absorption-free short-wavelength data set as reference data set for scaling is required. At even longer wavelengths it is very likely that new approaches are needed. This may even include an experimental or an analytical absorption correction.

Another way to experimentally minimize difficulties arising from absorption is to make any crystal sample absorption systematic error the same for anomalous difference pairs. For instance, the crystal can be perfectly aligned across the crystal-mounting axis, so that the Friedel pairs are measured at the same time and on the same image. This was for instance followed by Einspahr *et al.* (1985) for their experiment on pea lectin (see above) using the goniometer head arcs to set the crystal axes. Generally, such an approach requires a four-circle set-up or a κ-goniometer, which many synchrotron MX beamlines are not equipped with. Without such a possibility, one may think of including the time differences between Friedel pairs, which result from the degree of misalignment from the perfect sample setting (Nieh & Helliwell, 1995) as additional information into the scaling stage.

Especially at higher-energy sources in cases when Si(111) is used as a monochromator, the appearance of reflections originating from the third harmonic wavelength constitutes another problem. An easy solution to that would be to de-tune the second monochromator crystal at the expense of some of the incident intensity. This approach works satisfactorily at least up to wavelengths of about 2.6 Å at Elettra (Weiss, Sicker & Hilgenfeld, 2001). For even longer wavelengths it may become mandatory to insert an extra mirror into the beamline in order to cut the high-energy parts of the wavelength spectrum appropriately.

7. Conclusion and outlook

In summary, it could be shown that the longer wavelengths (1.5–3.0 Å) are accessible at many MX beamlines across Europe, and that experiments at these wavelengths can be undertaken almost routinely. Developments such as the Elettra HePBP will almost certainly improve the data, although the experiment itself will become a bit more difficult. κ-Geometry has not been extensively discussed in the text of this review, because most synchrotron MX beamlines do not provide κ-geometry as an option. It has to be expected, however, that this will change in the future, because it is clear that κ-geometry will contribute to the data quality, especially in those cases where the treatment of absorption will remain to rely on the scaling and merging step.

Diffraction experiments at long wavelengths (>3.0 Å) are still in their infancy state, but it can be expected that developments over the next few years with respect to diffractometers, detectors and crystal mounting will also make these experiments more feasible. Strong anomalous diffraction can then be observed near the absorption edges of S and P,

elements that are intrinsically present in biological macro-molecules. In addition, especially in the case of sulfur, the distinction between different chemical states (from -2 to $+6$) by anomalous scattering can be achieved.

References

Anderson, D. H., Weiss, M. S. & Eisenberg, D. (1996). *Acta Cryst.* D**52**, 469–480.

Arndt, U. W. (1984). *J. Appl. Cryst.* **17**, 118–119.

Behrens, W., Otto, H., Stuhrmann, H. B. & Heyn, M. P. (1998). *Biophys. J.* **75**, 255–263.

Biou, V., Boesecke, P., Bois, J.-M., Brandolin, G., Kahn, R., Mas, C., Nauton, L., Nury, H., Pebay-Peyroula, E., Vicat, J. & Stuhrmann, H. B. (2005). *J. Synchrotron Rad.* **12**, 402–409.

Blow, D. M. (1958). *Proc. R. Soc. A*, pp. 302–336.

Brown, J., Esnouf, R. M., Jones, M. A., Linnell, J., Harlos, K., Hassan, A. B. & Jones, E. Y. (2002). *EMBO J.* **21**, 1054–1062.

Carpentier, P., Berthet-Colominas, C., Capitan, M., Chesne, M.-L., Fanchon, E., Lequien, S., Stuhrmann, H., Thiaudière, D., Vicat, J., Zielinski, P. & Kahn, R. (2000). *Cell. Mol. Biol.* **46**, 915–935.

Carpentier, P., Boesecke, P., Bois, J.-M., Chesne, M.-L., Fanchon, E., Kahn, R., Stuhrmann, H. & Vicat, J. (2002). *Acta Phys. Pol.* **101**, 603–612.

Chesne, M.-L. (2002). Thesis, Université Joseph Fourier, Grenoble, France.

Cianci, M., Antonyuk, S., Bliss, N., Buffey, S. G., Cheung, K. C., Clarke, J. A., Derbyshire, G. E., Ellis, M. J., Enderby, M. J., Grant, A. F., Holbourn, M. P., Laundy, D., Nave, C., Ryder, R., Stephenson, P., Helliwell, J. R. & Hasnain, S. S. (2005). *J. Synchrotron Rad.* Submitted.

Cianci, M., Rizkallah, P. J., Olczak, A., Raftery, J., Chayen, N. E., Zagalsky, P. F. & Helliwell, J. R. (2001). *Acta Cryst.* D**57**, 1219–1229.

Dauter, Z. & Adamiak, D. A. (2001). *Acta Cryst.* D**57**, 990–995.

Dauter, Z., Dauter, M., de La Fortelle, E., Bricogne, G. & Sheldrick, G. M. (1999). *J. Mol. Biol.* **289**, 83–92.

Dauter, Z., Dauter, M. & Rajashankar, K. R. (2000). *Acta Cryst.* D**56**, 232–237.

Debreczeni, J. E., Bunkoczi, G., Ma, Q., Blaser, H. & Sheldrick, G. M. (2003). *Acta Cryst.* D**59**, 688–696.

Duke, E. M. H. (2004). BCA Spring Meeting Conference Abstracts, Manchester, UK.

Einspahr, H., Suguna, K., Suddath, F. L., Ellis, G., Helliwell, J. R. & Papiz, M. Z. (1985). *Acta Cryst.* B**41**, 336–341.

Evans, G. & Bricogne, G. (2002). *Acta Cryst.* D**58**, 976–991.

Evans, G. & Bricogne, G. (2003). *Acta Cryst.* D**59**, 1923–1929.

Evans, G., Polentarutti, M., Djinović Carugo, K. & Bricogne, G. (2003). *Acta Cryst.* D**59**, 1429–1434.

Ferreira, K. N., Iverson, T. M., Maghlaoui, K., Barber, J. & Iwata, S. (2004). *Science*, **303**, 1831–1838.

Fourme, R., Shepard, W., Kahn, R., L'Hermite, G. & Li De La Sierra, I. (1995). *J. Synchrotron Rad.* **2**, 36–48.

Gordon, E. J., Leonard, G. A., McSweeney, S. & Zagalsky, P. F. (2001). *Acta Cryst.* D**57**, 1230–1237.

Helliwell, J. R. (1984). *Rep. Prog. Phys.* **47**, 1403–1497.

Helliwell, J. R. (1993). *Daresbury CCP4 Study Weekend Proceedings* DL/Sci/R34, pp. 80–88. CCLRC Daresbury Laboratory, Warrington, UK.

Helliwell, J. R. (2004). *J. Synchrotron Rad.* **11**, 1–3.

Helliwell, J. R., Ealick, S., Doing, P., Irving, T. & Szebenyi, M. (1993). *Acta Cryst.* D**49**, 120–128.

Hendrickson, W. A. (1999). *J. Synchrotron Rad.* **6**, 845–851.

Hendrickson, W. A. & Ogata, C. M. (1997). *Methods Enzymol.* **276**, 494–523.

Hendrickson, W. A., Smith, J. L., Phizackerley, R. P. & Merritt, E. A. (1988). *Proteins*, **4**, 77–88.

Hendrickson, W. A. & Teeter, M. M. (1981). *Nature (London)*, **290**, 107–113.

Kuettner, E. B., Hilgenfeld, R. & Weiss, M. S. (2002). *J. Biol. Chem.* **277**, 46402–46407.

Kwiatkowski, W., Noel, J. P. & Choe, S. (2000). *J. Appl. Cryst.* **33**, 876–881.

Lehmann, M. S., Müller, H.-H. & Stuhrmann, H. B. (1993). *Acta Cryst.* D**49**, 308–310.

Li, S., Finley, J., Liu, Z. J., Qiu, S. H., Chen, H., Luan, C. H., Carson, M., Tsao, J., Johnson, D., Lin, G., Zhao, J., Thomas, W., Nagy, L. A., Sha, B., DeLucas, L. J., Wang, B. C. & Luo, M. (2002). *J. Biol. Chem.* **277**, 48596–48601.

Liu, Y., Ogata, C. M. & Hendrickson, W. A. (2001). *Proc. Natl. Acad. Sci. USA*, **98**, 10648–10653.

Liu, Z.-J., Vysotski, E. S., Chen, C.-J., Rose, J. P., Lee, J. & Wang, B.-C. (2000). *Protein Sci.* **9**, 2085–2093.

Miao, J. W., Hodgson, K. O. & Sayre, D. (2001). *Proc. Natl. Acad. Sci. USA*, **98**, 6641–6645.

Micossi, E., Hunter, W. N. & Leonard, G. A. (2002). *Acta Cryst.* D**58**, 21–28.

Mueller-Dieckmann, C., Polentarutti, M., Djinović Carugo, K., Panjikar, S., Tucker, P. A. & Weiss, M. S. (2004). *Acta Cryst.* D**60**, 28–38.

Murray, J. W., Garman, E. F. & Ravelli, R. B. G. (2004). *J. Appl. Cryst.* **37**, 513–522.

Murthy, H. M., Hendrickson, W. A., Orme-Johnson, W. H., Merritt, E. A. & Phizackerley, R. P. (1988). *J. Biol. Chem.* **263**, 18430–18436.

Nieh, Y. P. & Helliwell, J. R. (1995). *J. Synchrotron Rad.* **2**, 79–82.

Olsen, O., Flensburg, C., Olsen, O., Bricogne, G. & Henriksen, A. (2004). *Acta Cryst.* D**60**, 250–255.

Phillips, J. C. & Hodgson, K. O. (1980). *Synchrotron Radiation Research*, pp. 565–605, edited by H. Winick and S. Doniach. New York/London: Plenum.

Polentarutti, M., Glazer, R. & Djinović Carugo, K. (2004). *J. Appl. Cryst.* **37**, 319–324.

Polikarpov, I. (1997). *J. Synchrotron Rad.* **4**, 17–20.

Polikarpov, I., Teplyakov, A. & Oliva, G. (1997). *Acta Cryst.* D**53**, 734–737.

Ramagopal, U. A., Dauter, M. & Dauter, Z. (2003). *Acta Cryst.* D**59**, 1020–1027.

Ramin, M., Shepard, W., Fourme, R. & Kahn, R. (1999). *Acta Cryst.* D**55**, 157–167.

Ravelli, R. B., Leiros, H. K., Pan, B., Caffrey, M. & McSweeney, S. (2003). *Structure*, **11**, 217–224.

Sauer, O., Roth, M., Schirmer, T., Rummel, G. & Kratky, C. (2002). *Acta Cryst.* D**58**, 60–69.

Schiltz, M., Kvick, Å., Svensson, O. S., Shepard, W., de La Fortelle, E., Prangé, T., Kahn, R., Bricogne, G. & Fourme, R. (1997). *J. Synchrotron Rad.* **4**, 287–297.

Scholl, G., Dauvergne, F., Gabriel, A., Hütsch, M., Marmotti, M., Sayers, S., Stuhrmann, S., Thomas, J., Trame, C. & Stuhrmann, H. B. (1995). *Nucl. Instrum. Methods*, B**97**, 303–307.

Schuermann, J. P. & Tanner, J. J. (2003). *Acta Cryst.* D**59**, 1731–1736.

Sekar, K., Rajakannan, V., Velmurugan, D., Yamane, T., Thirumurugan, R., Dauter, M. & Dauter, Z. (2004). *Acta Cryst.* D**60**, 1586–1590.

Smith, J. L., Hendrickson, W. A. & Addison, A. W. (1983). *Nature (London)*, **303**, 86–88.

Stuhrmann, S. (1997). Thesis, University of Hamburg, Germany.

Stuhrmann, S., Bartels, K. S., Braunwarth, W., Doose, R., Dauvergne, F., Gabriel, A., Knöchel, A., Marmotti, M., Stuhrmann, H. B., Trame, C. & Lehmann, M. S. (1997). *J. Synchrotron Rad.* **4**, 298–310.

Stuhrmann, S., Bartels, K. S., Hütsch, M., Marmotti, M., Sayers, Z., Thomas, J., Trame, C. & Stuhrmann, H. B. (1996). *Structural Studies of Crystals*, pp. 276–288. Moscow: Nauka Fizmatlit. (In Russian.)

Stuhrmann, S., Hütsch, M., Trame, C., Thomas, J. & Stuhrmann, H. B. (1995). *J. Synchrotron Rad.* **2**, 83–86.

Teplyakov, A., Oliva, G. & Polikarpov, I. (1998). *Acta Cryst.* D**54**, 610–614.

Thomas, J. (1997). Thesis, University of Hamburg, Germany.

Trame, C. (1997). Thesis, University of Hamburg, Germany.

Wang, B.-C. (1985). *Methods Enzymol.* **115**, 90–112.

Weiss, M. S. (2001). *J. Appl. Cryst.* **34**, 130–135.

Weiss, M. S., Mander, G., Hedderich, R., Diederichs, K., Ermler, U. & Warkentin, E. (2004). *Acta Cryst.* D**60**, 686–695.

Weiss, M. S., Panjikar, S., Nowak, E. & Tucker, P. A. (2002). *Acta Cryst.* D**58**, 1407–1412.

Weiss, M. S., Sicker, T., Djinović Carugo, K. & Hilgenfeld, R. (2001). *Acta Cryst.* D**57**, 689–695.

Weiss, M. S., Sicker, T. & Hilgenfeld, R. (2001). *Structure*, **9**, 771–777.

Xia, D., Yu, C. A., Kim, H., Xia, J. Z., Kachurin, A. M., Zhang, L., Yu, L. & Deisenhofer, J. (1997). *Science*, **277**, 60–66. Erratum: *Science* (1997). **278**, 2037.

Yang, C. & Pflugrath, J. W. (2001). *Acta Cryst.* D**57**, 1480–1490.

Yang, C., Pflugrath, J. W., Courville, D. A., Stence, C. N. & Ferrara, J. D. (2003). *Acta Cryst.* D**59**, 1943–1957.